Electromagnetic field near rough surfaces of spatially dispersive systems

Shu Wang and Rubén G. Barrera

Instituto de Física, Universidad Nacional Autónoma de México, Apartado Postal 20-364,
01000 México, Distrito Federal, Mexico

W. Luis Mochán

Laboratorio de Cuernavaca, Instituto de Física, Universidad Nacional Autónoma de México, Apartado Postal 139-B,
62191 Cuernavaca, Morelos, Mexico

The Rayleigh-Fano method and a hydrodynamic model have been used to study the electromagnetic field near a rough surface bounding a nonlocal conductor for both *p*- and *s*-polarized incident waves. Nonlocality is accounted for by including longitudinal electromagnetic waves and using additional boundary conditions. A formal perturbative solution has been derived to arbitrary order in the amplitude of the roughness profile. We apply these formal solutions to an explicit first- and second-order calculation of the diffracted fields and the reflectance of a periodic grating. Numerical results are given for both local and nonlocal media, yielding significant differences, which are discussed.

I. INTRODUCTION

In recent years, there has been an increasing number of theoretical[1-6] and experimental[7-9] investigations on the optical properties of surfaces that are not perfectly flat. A number of intriguing physical phenomena such as the surface-enhanced Raman signal produced by molecules adsorbed on metal surfaces,[10-16] the enhancement of second-harmonic generation in reflection from a metal surface,[17-20] and light emission by tunnel junctions[21-24] require the presence of roughness to be observed. Most of the theoretical work on rough surfaces has been done by considering a local dielectric response of the metal. In this case the Rayleigh-Fano method[25] has been successfully applied not only to small-amplitude rough surfaces but also to large-amplitude ones, where the method was not expected to be valid. In the latter case, the use of the extinction theorem has been essential to achieve rapid convergence.[26] The type of convergence that is attained in large-amplitude roughness is still a matter of debate.[26-31]

On the other hand, the treatment of a nonplanar surface with a nonlocal (spatially dispersive) dielectric response has not been thoroughly explored. One would expect nonlocal effects[32-42] to become important if the diffracted fields has a short length scale of variation, as in metallic gratings with spatial periods of the order of 100 Å or less. An extreme example of this type of grating is the reconstructed face of some metallic crystals[43] where the spatial period is of only a few angstroms.

In this paper we develop a perturbative formalism based on the Rayleigh-Fano method for the scattering of an electromagnetic wave by a rough metal which is described by a nonlocal hydrodynamic longitudinal dielectric function[44,45]

$$\epsilon_l(\omega,\mathbf{k})=\epsilon_b(\omega)=\frac{\omega_p^2}{\omega^2+i\omega/\tau-\beta^2 k^2} \tag{1a}$$

and a local transverse response

$$\epsilon_t(\omega)=\epsilon_b(\omega)-\frac{\omega_p^2}{\omega^2+i\omega/\tau} . \tag{1b}$$

Here ω is the frequency, ω_p is the plasma frequency for the conduction-electron gas, τ is its electronic lifetime, $\epsilon_b(\omega)$ is the contribution of the bound electrons to the dielectric response, $\mathbf{k}$ is the wave vector, and $\beta^2=\frac{3}{5}v_F^2$ is the stiffness parameter, where v_F is the Fermi velocity.

The response (1a) implies the presence of longitudinal electromagnetic waves whose wave vector l obeys the dispersion relation

$$\epsilon_l(\omega,l)=0 , \tag{2}$$

in addition to the usual transverse waves. As is well known, the matching of all the field amplitudes across the surface requires additional boundary conditions (ABC's).[46-49] These have usually been applied at a flat surface; in this paper we solve the hydrodynamic model, but impose the usual electromagnetic boundary conditions and the ABC's at the surface of a rough metal.

The hydrodynamic model is known to have many shortcomings for flat surfaces:[50] it does not account for electron-hole pair excitations and it assumes an unrealistic discontinuity in the electronic density at the surface. We do not expect these effects to be less important at rough surfaces. However it has not been possible yet to apply microscopic calculations[51] in the presence of roughness and the extension[52] of the semiclassical infinite barrier model has some unsatisfactory features. The hydrodynamic model includes some nonlocal effects, such as

the existence of longitudinal modes and their coupling to transverse waves at surfaces, and it leads to a well-posed problem at rough surfaces, so we believe that its solution is an important step in the understanding of nonlocal effects at nonideal surfaces.

The outline of the paper is as follows. In Sec. II, we extend the Rayleigh-Fano theory to nonlocal systems within a perturbative approach and we obtain an iterative expression for the scattered fields to all orders in the profile amplitude. Then we apply the results to the calculation of the scattered fields and the reflectance of a sinusoidal metallic grating up to second order. Our results and their comparison with the local theory are shown in Sec. III, and Sec. IV is devoted to conclusions.

II. THEORY

In this section we solve the boundary-value problem for an electromagnetic plane wave with arbitrary polarization incident upon a surface defined by the equation

$$f(x,y,z) \equiv z - h\xi(x,y) = 0 \ . \tag{3}$$

We assume that the region $z > h\xi(x,y)$ is characterized by the dielectric functions ϵ_t and ϵ_l given by Eq. (1) and the region $z < h\xi(x,y)$ is vacuum. We will treat h as a small parameter in the perturbative solution of the problem.

The unit vector $\hat{n}$ directed normally outward from the surface is given by

$$\hat{n}(\xi) = \frac{\nabla f}{|\nabla f|} = \frac{(-h\xi_x, -h\xi_y, 1)}{[(h\xi_x)^2 + (h\xi_y)^2 + 1]^{1/2}} \ , \tag{4}$$

where ξ_x and ξ_y denote the partial derivatives of $\xi(x,y)$ with respect to x and y. The wave vectors of the incident, reflected, and transmitted waves are denoted by

$$\mathbf{q}_i = (Q_{xi}, Q_{yi}, q_{zi}) \ , \tag{5a}$$

$$\mathbf{q} = (Q_x, Q_y, -q_z) \ , \tag{5b}$$

$$\mathbf{k} = (Q_x, Q_y, k_z) \ , \tag{5c}$$

where $q_z^2 = \omega^2/c^2 - Q^2$, $k_z^2 = \epsilon_t \omega^2/c^2 - Q^2$, and $Q = (Q_x, Q_y, 0)$.

The transmitted electric and magnetic fields are decomposed into s ($\mathbf{E}_{st}$ and $\mathbf{B}_{st}$) and p ($\mathbf{E}_{pt}$ and $\mathbf{B}_{pt}$) polarized components:

$$\mathbf{E}_{st}(\mathbf{Q}) = S_t e^{i(Q_x x + Q_y y + k_z z)}(-Q_y, Q_x, 0) \ , \tag{6a}$$

$$\mathbf{B}_{st}(\mathbf{Q}) = \frac{c}{\omega} S_t e^{i(Q_x x + Q_y y + k_z z)}(-k_z Q_x, -k_z Q_y, Q^2) \ , \tag{6b}$$

$$\mathbf{E}_{pt}(\mathbf{Q}) = \frac{c}{\epsilon_t \omega} P_t e^{i(Q_x x + Q_y y + k_z z)}(k_z Q_x, k_z Q_y, -Q^2) \ , \tag{6c}$$

and

$$\mathbf{B}_{pt}(\mathbf{Q}) = P_t e^{i(Q_x x + Q_y y + k_z z)}(-Q_y, Q_x, 0) \ . \tag{6d}$$

Similar expressions can be written for the incident

(reflected) field(s) by setting $\epsilon_t = 1$ and replacing k_z by q_{zi} ($-q_z$). We call $S_\alpha = S_\alpha(\mathbf{Q}, \omega)$ and $P_\alpha = P_\alpha(\mathbf{Q}, \omega)$, $\alpha = i, r, t$, the amplitude functions. Here and in the following we omit the explicit dependence on $\mathbf{Q}$ and ω and the real-space coordinates of this and other quantities unless it is inconvenient.

Within a spatially dispersive metal there are also longitudinal waves whose electric and magnetic fields are given by

$$\mathbf{E}_l(\mathbf{Q}) = L e^{i(Q_x x + Q_y y + l_z z)}(Q_x, Q_y, l_z) \ , \tag{7a}$$

$$\mathbf{B}_l(\mathbf{Q}) = 0 \ , \tag{7b}$$

where $l = (Q_x, Q_y, l_z)$ satisfies the dispersion relation given by Eq. (2) and $L = L(\mathbf{Q}, \omega)$ is the longitudinal amplitude function.

We choose the X-Z plane as the plane of incidence, i.e., $\mathbf{q}_i = (Q_{xi}, 0, q_{zi})$. Using the notation introduced above, the incident fields are given by

$$\mathbf{E}_i = \mathbf{E}_{si}(\mathbf{Q}_i) + \mathbf{E}_{pi}(\mathbf{Q}_i) \ , \tag{8a}$$

$$\mathbf{B}_i = \mathbf{B}_{si}(\mathbf{Q}_i) + \mathbf{B}_{pi}(\mathbf{Q}_i) \ , \tag{8b}$$

the reflected fields by

$$\mathbf{E}_r = \sum_{\mathbf{Q}'} [\mathbf{E}_{sr}(\mathbf{Q}') + \mathbf{E}_{pr}(\mathbf{Q}')] \ , \tag{8c}$$

$$\mathbf{B}_r = \sum_{\mathbf{Q}'} [\mathbf{B}_{sr}(\mathbf{Q}') + \mathbf{B}_{pr}(\mathbf{Q}')] \ , \tag{8d}$$

and the transmitted fields by

$$\mathbf{E}_t = \sum_{\mathbf{Q}'} [\mathbf{E}_{st}(\mathbf{Q}') + \mathbf{E}_{pt}(\mathbf{Q}') + \mathbf{E}_{lt}(\mathbf{Q}')] \ , \tag{8e}$$

$$\mathbf{B}_t = \sum_{\mathbf{Q}'} [\mathbf{B}_{st}(\mathbf{Q}') + \mathbf{B}_{pt}(\mathbf{Q}')] \ . \tag{8f}$$

Now we proceed to establish the boundary conditions which have to be fulfilled at the interface $z = h\xi(x,y)$. Two of them follow from Maxwell's equations; they are the continuity across the interface of the tangential projection of $\mathbf{E}$ and $\mathbf{B}$,

$$\mathbf{F} = \mathbf{E} - (\hat{n} \cdot \mathbf{E})\hat{n} \ , \tag{9a}$$

$$\mathbf{K} = \mathbf{B} - (\hat{n} \cdot \mathbf{B})\hat{n} \ . \tag{9b}$$

We choose as an additional boundary condition the continuity of

$$\mathbf{G} = (\hat{n} \cdot \epsilon_b \mathbf{E})\hat{n} \ , \tag{9c}$$

which corresponds to the continuity of the normal projection of the conduction-electron current.[46]

Of the nine continuous field components appearing in Eqs. (9) only five are independent. Choosing the x and y components of $\mathbf{F}$ and $\mathbf{K}$, the z component of $\mathbf{G}$, and using Eq. (8), we write the continuity conditions in matrix form as

$$\sum_{\mathbf{Q}'} \mathsf{R}(\mathbf{Q}', \rho) \mathsf{W}(\mathbf{Q}', \rho) e^{i\mathbf{Q}' \cdot \rho} \mathsf{A}(\mathbf{Q}') = \mathsf{I}(\rho) e^{i\mathbf{Q}_i \cdot \rho} \ , \tag{10a}$$

which has to be solved for the amplitudes of the reflected and transmitted waves

$$A(Q') = \begin{bmatrix} S_r(Q') \\ S_t(Q') \\ P_r(Q') \\ P_t(Q') \\ L(Q') \end{bmatrix} . \qquad (10b)$$

Here $\rho = (x,y)$, the five-dimensional vector $I(\rho)$ characterizes the incident fields, the 5×5 matrix $R(Q',\rho)$ depends on the local orientation $\hat{n}$ of the surface while the matrix $W(Q',\rho)$ has the information on the height $h\xi(\rho)$. Explicit expressions for I, R, and W are given in Appendix A.

Now we perform an expansion of all quantities in Eq. (10a) in powers of h

$$R(Q',\rho) = \sum_{j,k} R^{(jk)}(Q')\xi_x^j(\rho)\xi_y^k(\rho)h^{j+k} , \qquad (11a)$$

$$W(Q',\rho) = \sum_l W^{(l)}(Q')\xi^l(\rho)h^l , \qquad (11b)$$

$$I(\rho) = \sum_{j,k} I^{(jk)}\xi_x^j(\rho)\xi_y^k(\rho)h^{j+k} , \qquad (11c)$$

$$A(Q') = \sum_m A^{(m)}(Q')h^m . \qquad (11d)$$

Notice that we extracted from $R(Q',\rho)$, $W(Q',\rho)$, and $I(\rho)$ all the shape-dependent information, so that $R^{(jk)}(Q')$, $W^{(l)}(Q')$, and $I^{(jk)}$ are independent of the surface profile. Substituting Eq. (11) in Eq. (10a) and taking a Fourier transform, we obtain

$$\sum_{Q'} \sum_{j,k,l,m \geq 0} \zeta^{jkl}(Q-Q')R^{(jk)}(Q')W^{(l)}(Q')A^{(m)}(Q')h^{j+k+l+m} = \sum_{j,k} \zeta^{jk0}(Q-Q_i)I^{(jk)}h^{j+k} , \qquad (12)$$

where we defined the Fourier transform through

$$F(Q) \equiv \frac{1}{A} \int F(\rho)e^{-iQ\cdot\rho}d^2\rho , \qquad (13)$$

with A the area of the nominal $(z=0)$ surface, and $\zeta^{jkl}(Q)$ is the Fourier transform of

$$\zeta^{jkl}(\rho) \equiv \xi_x^j(\rho)\xi_y^k(\rho)\xi^l(\rho) . \qquad (14)$$

Now we equate the coefficients of equal power of h in both sides of Eq. (12) and noticing that $W^{(0)}(Q')=1$ and that $\zeta^{000}(Q'-Q)=\delta_{Q,Q'}$, which corresponds to the conservation of the parallel projection of the momentum at a flat surface, we solve Eq. (12) for $A^{(n)}(Q)$ iteratively,

$$A^{(n)}(Q) = [R^{(00)}(Q)]^{-1}\left[\sum_{\substack{0 \leq j \leq n \\ k=n-j}} \zeta^{jk0}(Q-Q_i)I^{(jk)} - \sum_{Q'} \sum_{\substack{j,k,l \geq 0 \\ n \geq j+k+l > 0}} \zeta^{jkl}(Q-Q')R^{(jk)}(Q')W^{(l)}(Q')A^{(n-j-k-l)}(Q') \right] . \qquad (15)$$

Notice that in order to solve the problem to an arbitrary order in h, it is only necessary to invert the 5×5 matrix $R^{(00)}(Q)$. This is equivalent to solving the problem of dispersion of light incident with a parallel wave vector Q upon a flat surface. Furthermore, since p-polarized and longitudinal waves are uncoupled to s-polarized waves at a flat surface, the problem is further reduced to the separate inversion of the 3×3 submatrix which corresponds to the electric field in the plane of incidence, and the 2×2 submatrix which corresponds to the electric field normal to the plane of incidence. Analytic expressions for these inverses are readily obtained.

To illustrate this solution procedure, we choose a simple sinusoidal profile, that is,

$$z = h\xi(x,y) = h\cos(g\cdot\rho) . \qquad (16)$$

For simplicity, we choose $g = (g,0,0)$ parallel to Q_i, so there is no mixing between s- and p-polarized waves. Using Eqs. (15) and (16) we find that the amplitudes of the diffracted field are given to zeroth order by

$$A^{(0)}(Q) = [R^{(00)}(Q)]^{-1}I^{(00)}\delta_{Q,Q_i} , \qquad (17)$$

to first order by

$$A^{(1)}(Q) = \tfrac{1}{2}[R^{(00)}(Q)]^{-1}\{ig[I^{(10)} - R^{(10)}(Q_i)A^{(0)}(Q_i)](\delta_{Q,Q_i+g} - \delta_{Q,Q_i-g})$$
$$- R^{(00)}(Q_i)W^{(1)}(Q_i)A^{(0)}(Q_i)(\delta_{Q,Q_i+g} + \delta_{Q,Q_i-g})\} , \qquad (18)$$

and to second order by

$$A^{(2)}(Q) = -\tfrac{1}{4}[R^{(00)}(Q)]^{-1}\{g^2[I^{(20)} - R^{(20)}(Q_i)A^{(0)}(Q_i)](\delta_{Q,Q_i+2g} - 2\delta_{Q,Q_i} + \delta_{Q,Q_i-2g})$$
$$+ R^{(00)}(Q_i)W^{(2)}(Q_i)A^{(0)}(Q_i)(\delta_{Q,Q_i+2g} + 2\delta_{Q,Q_i} + \delta_{Q,Q_i-2g})$$
$$+ igR^{(10)}(Q_i)W^{(1)}(Q_i)A^{(0)}(Q_i)(\delta_{Q,Q_i+2g} - \delta_{Q,Q_i-2g})$$
$$+ 2igR^{(10)}(Q-g)A^{(1)}(Q-g) - 2igR^{(10)}(Q+g)A^{(1)}(Q+g)$$
$$+ 2R^{(00)}(Q-g)W^{(1)}(Q-g)A^{(1)}(Q-g) + 2R^{(00)}(Q+g)W^{(1)}(Q+g)A^{(1)}(Q+g)\} . \qquad (19)$$

Explicit expressions for $R^{(n0)}(\mathbf{Q}')$, $W^{(n)}(\mathbf{Q}')$, and $I^{(n0)}$ with $\mathbf{Q}'=(Q',0,0)$ are given in Appendix B for $n=0,1,2$.

The zeroth-order solution corresponds to the scattering by a flat surface. Clearly, the poles of $R^{(00)}(\mathbf{Q})^{-1}$ satisfy the dispersion relation of the surface plasmon polaritons (SPP) of a flat surface

$$\epsilon_t q_z(\mathbf{Q})+k_z(\mathbf{Q})+\frac{Q^2}{l_z(\mathbf{Q})}\left[1-\frac{\epsilon_t}{\epsilon_b}\right]=0 \ . \tag{20}$$

Thus from Eq. (18) we can see that the first-order solutions show resonant scattering at frequencies for which $\mathbf{Q}_i\pm\mathbf{g}$ satisfy Eq. (20). These first-order resonant solutions lie outside of the light cone; therefore, they are nonradiative in nature and they do not contribute directly to the reflected beam. Nevertheless they can be detected, for example, through the fields radiated by adsorbed molecules on the surface.[53] On the other hand, we can see from Eq. (19) that there is a second-order resonant contribution to the specularly reflected beam ($\mathbf{Q}=\mathbf{Q}_i$) which can be determined in reflectance experiments. These experiments are usually analyzed in terms of the differential reflectance, defined as

$$\frac{\Delta R}{R^{(0)}}\equiv\frac{R-R^{(0)}}{R^{(0)}} \ , \tag{21}$$

where R is the reflectance of the rough surface, and $R^{(0)}$ is the flat-surface reference.

In our case taking only into account contributions up to second order we obtain for p polarization

$$\frac{\Delta R_p}{R_p^{(0)}}=2h^2\mathrm{Re}\left[\frac{P_r^{(2)}}{P_r^{(0)}}\right] \ , \tag{22}$$

where $P_r^{(n)}$ is the amplitude function of the nth-order contributions to p-polarized reflected electric field [see Eq. (6c)].

In the local case the calculation follows the same procedure as above but without including the longitudinal wave, and therefore with no additional boundary condition. One is led to 4×4 matrix equations whose perturbative solution has exactly the same structure as Eqs. (17)–(19). It is worthwhile to point out that it is not convenient to obtain the local case as the $l\rightarrow i\infty$ limit of the nonlocal calculation, since in our perturbative approach we expand the fields in powers of $l\xi$ [see Eq. (A2)] and this causes convergence problems when the limit above is taken.[52] Since the details of local calculations have been already reported,[1] we will only show the numerical results in the next section, when we compare them with those of our nonlocal theory.

III. RESULTS

In this section we present numerical results for a sinusoidal metallic grating using the formulas derived above. From Eqs. (18) and (19) we can see that while there are no first-order specular beams and scattering occurs at $\mathbf{Q}=\mathbf{Q}_i\pm\mathbf{g}$, in second order there is one specular and two nonspecular beams with $\mathbf{Q}=\mathbf{Q}_i$, $\mathbf{q}_i\pm2\mathbf{g}$. There is

resonant scattering whenever the scattered wave vector $\mathbf{Q}$ or any of the intermediate wave vectors $\mathbf{Q}'$ [see Eq. (15)] satisfies the dispersion relation of the SPP [Eq. (20)] shown in Fig. 1. This figure was obtained by giving real values to ω, solving Eq. (20) for $\mathbf{Q}$ and plotting its real part. We used the dielectric response given by Eq. (1) with $\omega_p\tau=100$ and $\beta=0.003\,61c$, and we took $\epsilon_b=1$ for simplicity. For small $\mathbf{Q}$ ($Q\ll\omega_p/\beta$) there is no appreciable difference with the local case, which corresponds to $\beta=0$. The effects of nonlocality show up at large values of $\mathbf{Q}$ where there are significant deviations from the local result. This figure will be used to interpret the structure of the curves described below. In order to analyze our results for resonant scattering we define an enhancement factor as

$$r_1=\frac{1}{gh}\frac{|h\,\mathbf{E}_{pr}^{(1)}(\mathbf{Q}_i+\mathbf{g})|}{|\mathbf{E}_{pi}^{(0)}(\mathbf{Q}_i)|}$$

$$=\frac{|P_r^{(1)}(\mathbf{Q}_i+\mathbf{g})|}{g|P_i^{(0)}(\mathbf{Q}_i)|}\frac{[|q_z(\mathbf{Q}_i+\mathbf{g})|^2(Q_i+g)^2+(Q_i+g)^4]^{1/2}}{[|q_z(\mathbf{Q}_i)|^2Q_i^2+Q_i^4]^{1/2}}$$

$$\tag{23}$$

for the first-order fields, and

$$r_2=\frac{1}{(gh)^2}\frac{|h^2\mathbf{E}_{pr}^{(2)}(\mathbf{Q}_i)|}{|\mathbf{E}_{pi}^{(0)}(\mathbf{Q}_i)|}$$

$$=\frac{|P_r^{(2)}(\mathbf{Q}_i)|}{g^2|P_i^{(0)}(\mathbf{Q}_i)|} \tag{24}$$

for the second-order specular field, where we have introduced the expansion $\mathbf{E}=\sum_n h^n\mathbf{E}^{(n)}$. Notice that care must be exercised in the calculation of the absolute values
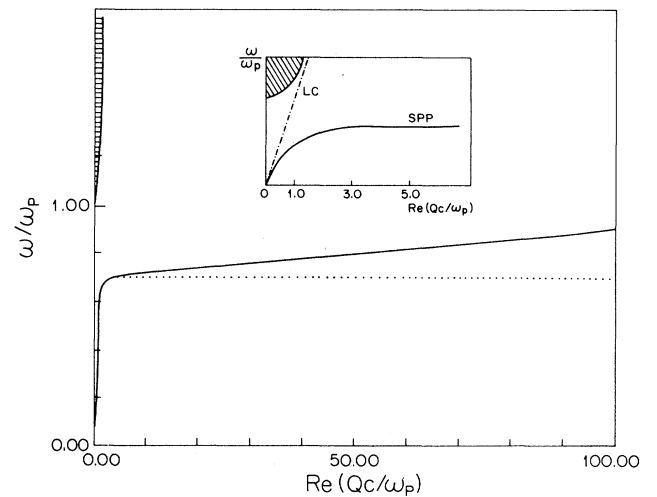

FIG. 1. Dispersion relation ω vs $\mathrm{Re}(Q)$ of the surface plasmon-polariton of a flat metal surface, calculated with a hydrodynamic (solid) and a local (dotted) model. The retarded region is enlarged in the inset. The dash-dotted line represents the light cone and the shadowed region is that in which the metal becomes transparent.

in Eq. (23) since the electric field might be a complex vector without a real direction. The dependence of the first- and second-order fields on h is divided out in the definitions of r_1 and r_2, and the scattering wave vector g is used to generate dimensionless quantities. Notice that r_1 is defined for scattering at $Q_i + g$; a similar expression holds for scattering at $Q_i - g$.

In Figs. 2, 3, and 4 we show local and nonlocal results for r_1 and r_2 as a function of g when the p-polarized light hits the surface at an angle $\theta = 30°$ for three different frequencies: $\omega/\omega_p = 0.4$, 0.5, and 0.8. The first-order non-local calculation shows a dip in Fig. 2 for a value of g which corresponds to a root of r_1. This is not strictly a zero because the roots are complex due to the finite value of τ. In the local case the zeros obey the relation

$$\epsilon_t Q_i (Q_i + g) - k_z (Q_i) k_z (Q_i + g) = 0 ,$$

which can be solved analytically and is displayed in the inset of Fig. 2, together with the roots that correspond to the nonlocal calculation which were obtained numerically. Notice that as $g \to \infty$ the local calculation approaches a finite frequency given by the smallest root of

$$\left[\frac{\omega}{\omega_p} \right]^4 - (2 \sin^2\theta + 1) \left[\frac{\omega}{\omega_p} \right]^2 + 1 = 0$$

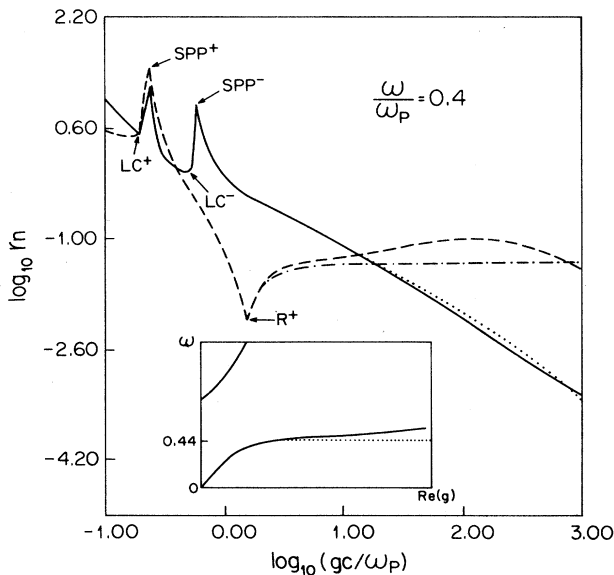(neglecting dissipation); this is not the case in the nonlo-

FIG. 3. Enhancement factor r_1 (dashed) and r_2 (solid) as a function of gc/ω_p for a fixed frequency $\omega/\omega_p = 0.5$. The corresponding local calculations are shown with dotted-dashed and dotted lines. The notation is as in Fig. 2. In the inset we show schematically the processes of SPP excitation at $Q_i + g$ or $Q_i - g$. The surface projection Q_i of the incident wave vector is represented by a dashed line through the origin inside the light cone (LC) and the nonplanar surface provides the additional momentum $\pm g$.

FIG. 2. Enhancement factor r_1 (dashed) and r_2 (solid) as a function of gc/ω_p for a fixed frequency $\omega/\omega_p = 0.4$. The corresponding local calculations are shown with dotted-dashed and dotted lines. The wave vectors g such that $Q_i \pm g$ lie on the SPP dispersion relation, on the light cone (LC), and the root (R) of the first-order scattered field are indicated. In the inset we show a schematic plot of the real part of the roots of r_1 as a function of ω; the solid line represents the nonlocal case while the dotted line represents the local one.
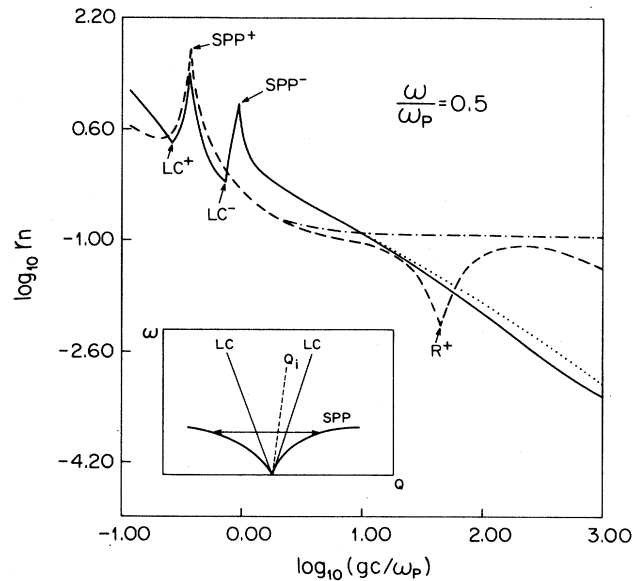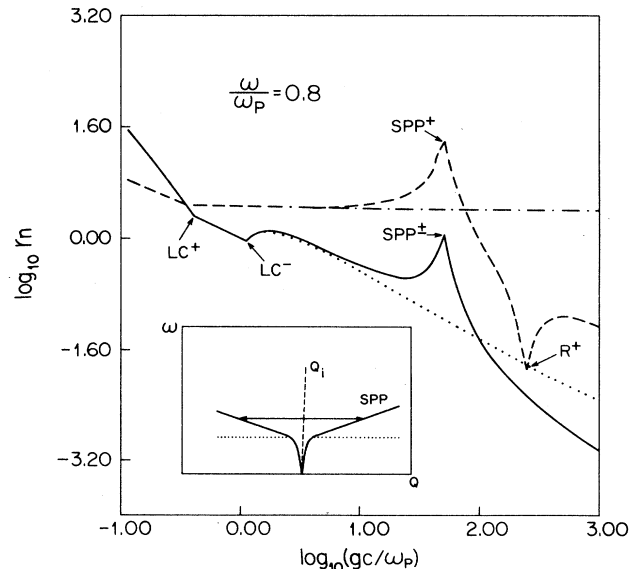

FIG. 4. Enhancement factor r_1 (dashed) and r_2 (solid) as a function of gc/ω_p for a fixed frequency $\omega/\omega_p = 0.8$. The corresponding local calculations are shown with dotted-dashed and dotted lines. The notation is as in Fig. 2. In the inset we show schematically the processes of SPP excitation at $Q_i + g$ or $Q_i - g$ which are possible in the nonlocal case only. The dotted line is the dispersion curve for local case.

cal calculation. It can be seen in the inset of Fig. 2 that for $\omega < 0.44\omega_p$ there are roots in both the local and non-local cases, while for $\omega > 0.44\omega_p$ there are roots only in the nonlocal case with large value of g. This behavior is also apparent in Figs. 3 and 4, where the nonlocal results show dips which are absent in the local case.

One of the most prominent features of Figs. 2 and 3 is the peak of r_1 due to SPP excitation at $Q_i + g$, and two peaks in r_2 due to SPP excitation at $Q_i \pm g$. In the insets of Figs. 3 and 4 we show schematically these two processes. As seen in Figs. 2 and 3, there is a noticeable difference between the results of the local and nonlocal calculations for high values of g. However, for small frequencies this difference is negligible around the SPP resonance. On the other hand, at $\omega/\omega_p > 1/\sqrt{2}$ (Fig. 4) there is no SPP peak at all in the local calculation while in the nonlocal case the resonant scattering by the SPP can be seen at large value of g. Since in this case $Q_i \ll g$, the two second-order peaks at $Q_i \pm g$ lie so close to each other that they cannot be discerned in the figure.

In Figs. 2, 3, and 4 we can also see one and two discontinuities in the slopes of r_1 and r_2, respectively. They correspond to values of g such that $Q_i \pm g$ lies on the surface of the light cone.

The structure in Figs. 5 and 6 corresponds to the features of Figs. 2–4: resonances when the scattered vectors $Q_i \pm g$ satisfy the SPP dispersion relation, slope
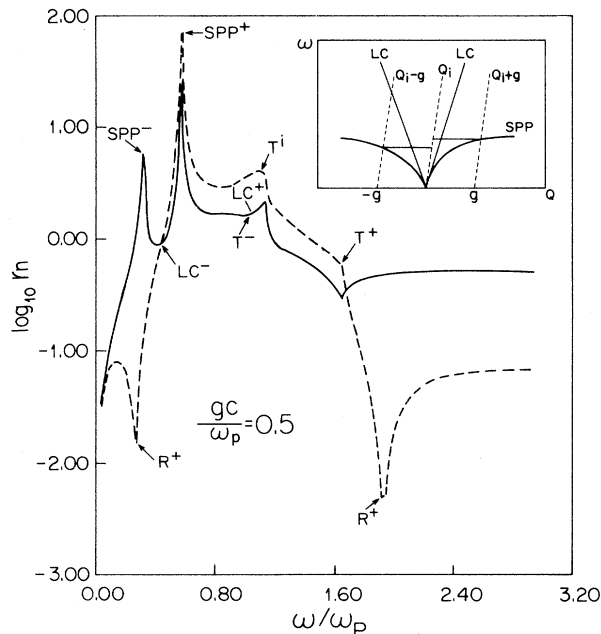

FIG. 6. Enhancement factor r_1 (dashed) and r_2 (solid) as a function of ω/ω_p for a fixed grating the wave vector $gc/\omega p = 100$. The corresponding local calculations are shown with dotted-dashed and dotted lines. The notation is as in Fig. 5. In the inset we show schematically the processes of the SPP excitation at $Q_i + g$ or $Q_i - g$ which correspond to two closely spaced values of ω. The dotted line is the dispersion curve for local case.

FIG. 5. Enhancement factor r_1 (dashed) and r_2 (solid) as a function of ω/ω_p for a fixed grating wave vector $gc/\omega_p = 0.5$. The frequencies for which the metal becomes transparent (T) for propagation with wave vectors Q_i and $Q_i \pm g$ are indicated. Otherwise, the notation is as in Fig. 2. In the inset we show schematically the processes of the SPP excitation at $Q_i + g$ or $Q_i - g$ which correspond to two different values of ω.
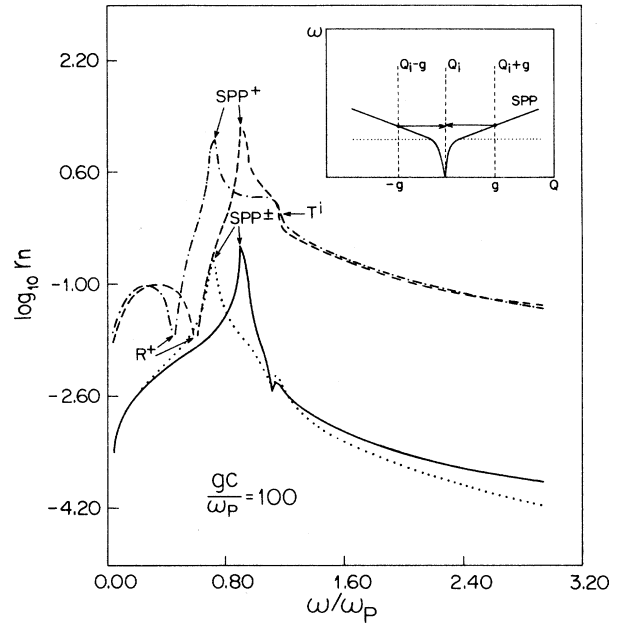
discontinuities when they intersect the light cone, and dips in the first-order calculations. These processes are illustrated by the insets of Figs. 5 and 6. There are also discontinuities in Figs. 5 and 6 whenever any of the reflected waves propagates at the critical angle $\theta_c = \arcsin\sqrt{\epsilon}$, at which the corresponding transmitted wave changes from evanescent to propagating; these discontinuities did not appear in Figs. 2–4 because there we chose $\omega < \omega_p$. Since the scattering wave vector is small in Fig. 5, the local and nonlocal results are very close to each other, while they differ considerably in Fig. 6 for which g approaches an atomic scale.

In Fig. 7 (8) we plot r_1 and r_2 versus gc/ω_p (ω/ω_p) for fixed value of $\omega/\omega_p = 0.5$ $(gc/\omega_p = 0.5)$ for the s-polarized light with the electric field along the grooves of the grating. In this case there is no mixing between s, p, and longitudinal waves, the local and the hydrodynamic results become identical, and there are no SPP resonances and no zeros in the first-order enhancement factor. The only structure visible in these figures consists of the slope discontinuities whose origin was discussed above.

In Fig. 9 we show the normalized change in reflectance $\Delta R/R$ versus ω/ω_p upon roughening [Eq. (21)] for a surface with microscopic scale roughness $(gc/\omega_p = 100)$ illuminated with p-polarized light [Eq. (22)] at the angle $\theta = 30°$. Note that the result was scaled with the pertur-

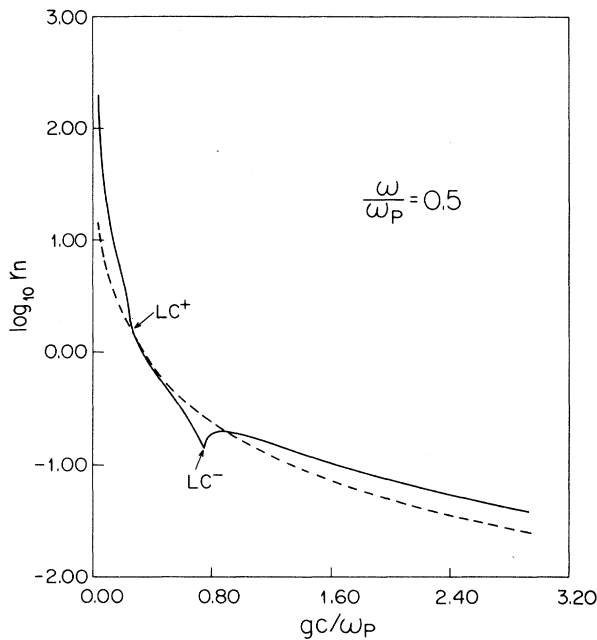FIG. 7. Enhancement factors r_1 (dashed) and r_2 (solid) for s-polarized field as a function of wave vector gc/ω_p for a fixed frequency $\omega/\omega_p = 0.5$.

bation parameter $(gh)^2$. The structure in this figure is closely correlated to that of Fig. 5 except for the peak at the Brewster frequency $\omega_B = \omega_p/(1 - \tan^2\theta) \approx 1.2\omega_p$ which arises from the zeros of $R^{(0)}$. The other large peak originates from the SPP resonance and its position is shifted significantly between the local ($\approx 0.71\omega_p$) and the
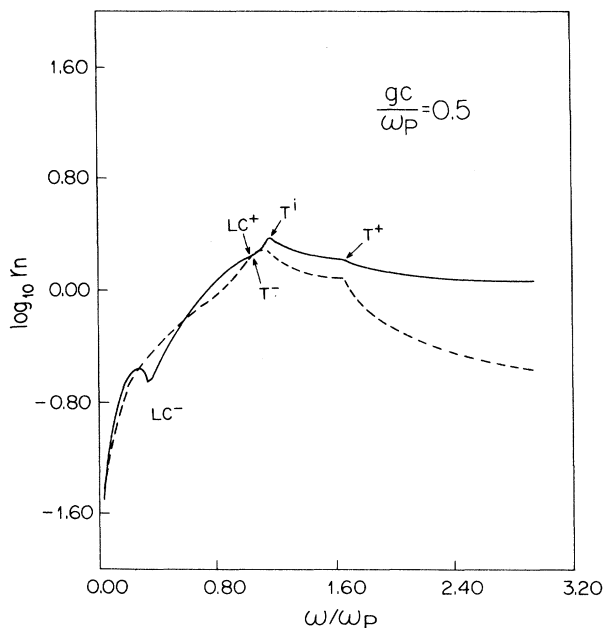

FIG. 8. Enhancement factor r_1 (dashed) and r_2 (solid) for s-polarized light as a function of frequency ω/ω_p for a fixed grating wave vector $gc/\omega_p = 0.5$.
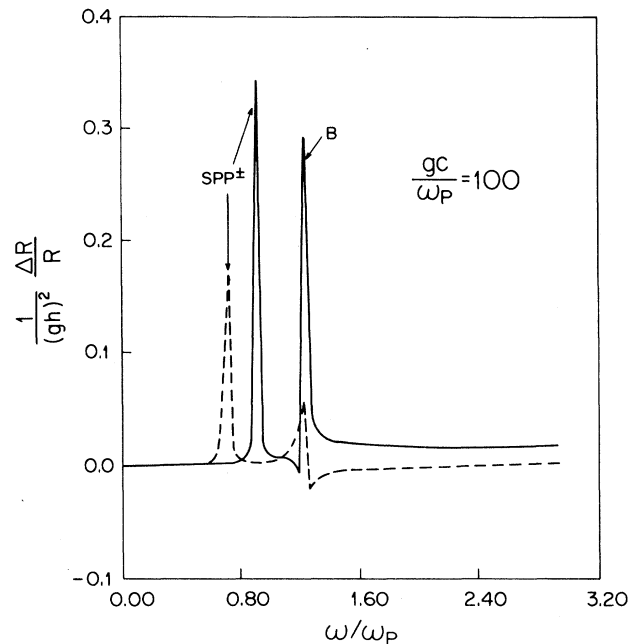

FIG. 9. Differential reflectance of p-polarized light as a function of frequency ω/ω_p for a fixed grating wave vector $gc/\omega_p = 100$, obtained through a local (dashed) and a nonlocal (solid) calculation. The positions of the SPP resonance and the Brewster (B) condition are indicated.

nonlocal ($\approx 0.9\omega_p$) calculations. Actually, in the local case this peak is quite insensitive to g while its position is nearly linear in g in the nonlocal case.

IV. CONCLUSIONS

In this work we have used the Rayleigh-Fano method to study the scattered fields near a rough metallic surface. Spatial dispersion was accounted for by using a hydrodynamic model complemented by an additional boundary condition. We have derived a formal perturbative solution to arbitrary order in the amplitude of the roughness for both nonlocal and local media. Our solution was applied to gratings and we obtained numerical results to first and second order. Our results display a very rich structure which was analyzed in terms of the bulk and surface modes of the corresponding flat system. The most noticeable structure stems from the excitation of the surface plasmon polariton which becomes possible due to the nonconservation of momentum along the surface. The position of the SPP resonance is shifted in the nonlocal calculation with respect to the local results, but its strength is not modified substantially. This result should be important in the analysis of surface-enhanced Raman scattering from surfaces with microroughness. We also found that under certain conditions the first-order diffracted fields are suppressed. These conditions are

very sensitive to spatial dispersion. As **g** increases, non-local effects become more important, and they must be incorporated in calculations involving systems whose roughness profile has characteristic lengths of the order of interatomic distances, as is the case for certain reconstructed metallic surfaces. Although not entirely realistic, our hydrodynamic calculation is the first one applied to metallic surfaces with small-scale roughness. Furthermore, the reflectance change upon roughening which we calculated to second order could be observed experimentally, for example, as an anisotropy in the reflectance of reconstructed (110) surfaces of noble metals.

APPENDIX A

In this appendix we give explicit expressions for the elements of the matrices $R(Q',\rho)$, $W(Q',\rho)$, and $I(\rho)$ which appear in Eq. (10a):

$$R_{11}(\mathbf{Q}',\rho) = -n_x n_y Q'_y - (1 - n_y^2)Q'_x \; ,$$

$$R_{12}(\mathbf{Q}',\rho) = (n_x n_y)Q'_y + (1 - n_y^2)Q'_x \; ,$$

$$R_{13}(\mathbf{Q}',\rho) = [-n_x n_y q'_z Q'_x + (1 - n_y^2)q'_z Q'_y - n_z n_y (Q')^2]c/\omega \; ,$$

$$R_{14}(\mathbf{Q}',\rho) = [-n_y n_x Q'_x (k'_z/\epsilon_t) + (1 - n_y^2)Q'_y(k'_z/\epsilon_t) + n_z n_y (Q')^2/\epsilon_t]c/\omega \; ,$$

$$R_{15}(\mathbf{Q}',\rho) = -n_x n_y Q'_x + (1 - n_y^2)Q'_y - n_z n_y l'_z \; ,$$

$$R_{21}(\mathbf{Q}',\rho) = [-(1 - n_x^2)q'_z Q'_x + n_y n_x q'_z Q'_y + n_z n_x (Q')^2]c/\omega \; ,$$

$$R_{22}(\mathbf{Q}',\rho) = [-(1 - n_x^2)k'_z Q'_x + n_y n_x k'_z Q'_y - n_z n_x (Q')^2]c/\omega \; ,$$

$$R_{23}(\mathbf{Q}',\rho) = (1 - n_x^2)Q'_y + n_y n_x Q'_x \; ,$$

$$R_{24}(\mathbf{Q}',\rho) = -(1 - n_x^2)Q'_y - n_y n_x Q'_x) \; ,$$

$$R_{25}(\mathbf{Q}',\rho) = 0 \; ,$$

$$R_{31}(\mathbf{Q}',\rho) = (1 - n_x^2)Q'_y + n_y n_x Q'_x \; ,$$

$$R_{32}(\mathbf{Q}',\rho) = -(1 - n_x^2)Q'_y - n_y n_x Q'_x \; ,$$

$$R_{33}(\mathbf{Q}',\rho) = [(1 - n_x^2)q'_z Q'_x - n_y n_x q'_z Q'_y - n_z n_x (Q')^2]c/\omega \; , \tag{A1}$$

$$R_{34}(\mathbf{Q}',\rho) = [(1 - n_x^2)Q'_x (k'_z/\epsilon_t) - n_y n_x Q'_y(k'_z/\epsilon_t) + n_z n_x (Q')^2/\epsilon_t]c/\omega \; ,$$

$$R_{35}(\mathbf{Q}',\rho) = (1 - n_x^2)Q'_x - n_y n_x Q'_y - n_z n_x l'_z \; ,$$

$$R_{41}(\mathbf{Q}',\rho) = [n_x n_y q'_z Q'_x - (1 - n_y^2)q'_z Q'_y + n_z n_y (Q')^2]c/\omega \; ,$$

$$R_{42}(\mathbf{Q}',\rho) = [n_x n_y k'_z Q'_x - (1 - n_y^2)k'_z Q'_y - n_z n_y (Q')^2]c/\omega \; ,$$

$$R_{43}(\mathbf{Q}',\rho) = -n_x n_y Q'_y - (1 - n_y^2)Q'_x \; ,$$

$$R_{44}(\mathbf{Q}',\rho) = (n_x n_y)Q'_y + (1 - n_y^2)Q'_x \; ,$$

$$R_{45}(\mathbf{Q}',\rho) = 0 \; ,$$

$$R_{51}(\mathbf{Q}',\rho) = n_x n_z Q'_y - n_y n_z Q'_x \; ,$$

$$R_{52}(\mathbf{Q}',\rho) = -n_x n_z \epsilon_b Q'_y + n_y n_z \epsilon_b Q'_x \; ,$$

$$R_{53}(\mathbf{Q}',\rho) = [n_x n_z q'_z Q'_x + n_y n_z q'_z Q'_y + n_z^2 (Q')^2]c/\omega \; ,$$

$$R_{54}(\mathbf{Q}',\rho) = [n_x n_z k'_z Q'_x + n_y n_z k'_z Q'_y - n_z^2 (Q')^2]\epsilon_b c/\epsilon_t \omega \; ,$$

$$R_{55}(\mathbf{Q}',\rho) = (n_x n_z Q'_x + n_y n_z Q'_y + n_z^2 l'_z)\epsilon_b \; ;$$

$$W(\mathbf{Q}',\rho) = \text{diag}(e^{-i(q'_z + q_{zi})\xi}, e^{i(k'_z - q_{zi})\xi}, e^{-i(q'_z + q_{zi})\xi}, e^{i(k'_z - q_{zi})\xi}, e^{i(l'_z - q_{zi})\xi}) \; , \tag{A2}$$

and

$$
\mathbf{I}(\rho) =
\begin{bmatrix}
(1-n_y^2)Q_iS_i + [(-n_xn_y)q_{zi}Q_ic/\omega + n_zn_yQ_i^2c/\omega]P_i \\
[(1-n_x^2)(-q_{zi}Q_ic/\omega) - n_zn_xQ_i^2c/\omega]S_i + (-n_yn_xQ_i)P_i \\
(-n_yn_xQ_i)S_i + [(1-n_x^2)q_{zi}Q_ic/\omega + n_zn_xQ_i^2c/\omega]P_i \\
[(-n_xn_y)(-q_{zi}Q_ic/\omega) - n_zn_yQ_i^2c/\omega]S_i + [(1-n_y^2)Q_i]P_i \\
(n_yn_zQ_i)S_i + (n_xn_zq_{zi}Q_ic/\omega - n_z^2Q_i^2c/\omega)P_i
\end{bmatrix} .
\tag{A3}
$$

APPENDIX B

In this appendix we give explicit expressions for the elements of the matrices $\mathsf{R}^{(n0)}(\mathbf{Q}')$, $\mathsf{W}^{(n)}(\mathbf{Q}')$, and $\mathsf{I}^{(n0)}$ for $\mathbf{Q}'=(Q',0,0)$ and $n=0,1,2$ which appear in Eqs. (17)–(19):

$$
\mathsf{R}^{(00)}(\mathbf{Q}') =
\begin{bmatrix}
-Q' & Q' & 0 & 0 & 0 \\
-cQ'q_z'/\omega & -cQ'k_z'/\omega & 0 & 0 & 0 \\
0 & 0 & cQ'q_z'/\omega & cQ'k_z'/\omega\epsilon_t & Q' \\
0 & 0 & -Q' & Q' & 0 \\
0 & 0 & c(Q')^2/\omega & -c(Q')^2\epsilon_b/\omega\epsilon_t & l_z'\epsilon_b
\end{bmatrix} ,
\tag{B1}
$$

$$
\mathsf{R}^{(10)}(\mathbf{Q}') =
\begin{bmatrix}
0 & 0 & 0 & 0 & 0 \\
-c(Q')^2/\omega & c(Q')^2/\omega & 0 & 0 & 0 \\
0 & 0 & c(Q')^2/\omega & -c(Q')^2/\omega\epsilon_t & l_z' \\
0 & 0 & 0 & 0 & 0 \\
0 & 0 & -q_z'cQ'/\omega & -ck_z'(Q')^2\epsilon_b/\omega\epsilon_t & -Q'\epsilon_b
\end{bmatrix} ,
\tag{B2}
$$

$$
\mathsf{R}^{(20)}(\mathbf{Q}') =
\begin{bmatrix}
0 & 0 & 0 & 0 & 0 \\
cQ'q_z'/\omega & cQ'k_z'/\omega & 0 & 0 & 0 \\
0 & 0 & -cQ'q_z'/\omega & -cQ'k_z'/\omega\epsilon_t & -Q' \\
0 & 0 & 0 & 0 & 0 \\
0 & 0 & -c(Q')^2/\omega & c(Q')^2\epsilon_b/\omega\epsilon_t & -l_z'\epsilon_b
\end{bmatrix} ,
\tag{B3}
$$

$$
\mathsf{W}^{(0)}(\mathbf{Q}') = 1 ,
\tag{B4}
$$

$$
\mathsf{W}^{(1)}(\mathbf{Q}') = \mathrm{diag}(-i(q_z'+q_{zi}), i(k_z'-q_{zi}), -i(q_z'+q_{zi}), i(k_z'-q_{zi}), i(l_z'-q_{zi})) ,
\tag{B5}
$$

$$
\mathsf{W}^{(2)}(\mathbf{Q}') = \mathrm{diag}(-\tfrac{1}{2}(q_z'+q_{zi})^2, -\tfrac{1}{2}(k_z'-q_{zi})^2, -\tfrac{1}{2}(q_z'+q_{zi})^2, -\tfrac{1}{2}(k_z'-q_{zi})^2, -\tfrac{1}{2}(l_z'-q_{zi})^2) ,
\tag{B6}
$$

$$
\mathsf{I}^{(00)} =
\begin{bmatrix}
Q_iS_i \\
-cq_{zi}Q_iS_i/\omega \\
cq_{zi}Q_iP_i/\omega \\
Q_iP_i \\
-cQ_i^2P_i/\omega
\end{bmatrix} ,
\tag{B7}
$$

$$
\mathsf{I}^{(10)} =
\begin{bmatrix}
0 \\
cQ_i^2S_i/\omega \\
-cQ_i^2P_i/\omega \\
0 \\
-cq_{zi}Q_iP_i/\omega
\end{bmatrix} ,
\tag{B8}
$$

and

$$
\mathbf{I}^{(20)} = \begin{bmatrix} 0 \\ cq_{zi}Q_iS_i/\omega \\ -cq_{zi}Q_iP_i/\omega \\ 0 \\ cQ_i^2P_i/\omega \end{bmatrix} .
$$

(B9)

[1] A. A. Maradudin, in *Surface Polaritons,* edited by V. M. Agranovich and D. L. Mills (North-Holland, Amsterdam, 1982), p. 405.

[2] N. E. Glass, M. Weber, and D. L. Mills, Phys. Rev. B **29**, 6548 (1984).

[3] G. A. Farias, A. A. Maradudin, and V. Celli, Surf. Sci. **129**, 9 (1983).

[4] E. Kröger and E. Kretschmann, Phys. Status Solidi B **76**, 515 (1976).

[5] O. Mata-Méndez and P. Halevi, Phys. Rev. B **36**, 1007 (1987).

[6] E. Kretschmann, T. L. Ferrel, and J. C. Ashley, Phys. Rev. Lett. **42**, 1312 (1979).

[7] R. Kötz, H. J. Lewerenz, and E. Kretschmann, Phys. Lett. **70A**, 452 (1979).

[8] K. J. Krane and H. Raether, Phys. Rev. Lett. **37**, 1355 (1976).

[9] W. L. Barnes and J. R. Sambles, Solid State Commun. **55**, 921 (1985).

[10] C. Y. Chen and E. Burstein, Phys. Rev. Lett. **45**, 1287 (1980).

[11] S. S. Jha, J. R. Kirtley, and J. C. Tsang, Phys. Rev. B **22**, 3973 (1980).

[12] D. J. Evan, S. Ushioda, and J. McMullen, Phys. Rev. Lett. **31**, 369 (1973).

[13] M. Nevière and R. Reinisch, Phys. Rev. B **26**, 5403 (1982).

[14] D. L. Mills and M. Weber, Phys. Rev. B **26**, 1075 (1982).

[15] R. M. Pierce and S. Ushioda, J. Phys. (Paris) Colloq. **45**, Suppl. 4, C5-230 (1984).

[16] G. S. Agarwal, Sudhanshu S. Jha, and J. C. Tsang, Phys. Rev. B **25**, 2089 (1982).

[17] G. S. Agarwal and S. S. Jha, Phys. Rev. B **26**, 482 (1982).

[18] C. K. Chen, A. R. B. de Castro, and Y. R. Shen, Phys. Rev. Lett. **46**, 145 (1981).

[19] A. Wokaun, J. G. Bergman, J. P. heritage, A. M. Glass, P. F. Liao, and D. H. Olson, Phys. Rev. B **24**, 849 (1981).

[20] G. A. Farias and a. A. Maradudin, Phys. Rev. B **30**, 3002 (1984).

[21] John Lambe and S. L. McCarthy, Phys. Rev. Lett. **37**, 923 (1976).

[22] J. R. Kirtley, T. N. Theis, and J. C. Tsang, Appl. Phys. Lett. **37**, 435 (1980).

[23] B. N. Kurdi and D. G. Hall, Opt. Commun. **51**, 303 (1984).

[24] N. E. Glass, D. L. Mills, and M. G. Weber, Phys. Rev. B **32**, 4919 (1985).

[25] Lord Rayleigh, Philos. Mag. **14**, 70 (1907); *Theory of Sound,* 2nd ed. (Dover, New York, 1945), Vol. II, p. 89.

[26] F. Toigo, A. Marvin, V. Celli, and N. R. Hill, Phys. Rev. B **15**, 5618 (1977).

[27] N. E. Glass and A. A. Maradudin, Phys. Rev. B **24**, 595 (1981).

[28] N. E. Glass, A. A. Maradudin, and V. Celli, Phys. Rev. B **26**, 5357 (1982).

[29] N. E. Glass and A. A. Maradudin, Surf. Sci. **114**, 240 (1982).

[30] B. Laks, D. L. Mills, and A. A. Maradudin, Phys. Rev. B **23**, 4965 (1981).

[31] N. R. Hill and V. Celli, Phys. Rev. B **17**, 2478 (1978).

[32] G. S. Agarwal, D. N. Pattanayak, and E. Wolf, Phys. Rev. B **11**, 1342 (1975).

[33] W. L. Schaich, Phys. Rev. B **31**, 3409 (1985).

[34] Denping Xue and Chien-hua Tsai, Solid State Commun. **56**, 651 (1985).

[35] G. Barton, J. Phys. C **19**, 975 (1986).

[36] G. Eliasson, G. F. Giulliani, J. J. Quinn, and R. F. Wallis, Phys. Rev. B **33**, 1406 (1986).

[37] K. L. Kliewer, Surf. Sci. **101**, 57 (1980).

[38] G. S. Agarwal, Solid State Commun. **43**, 99 (1982).

[39] W. Luis Mochán and Rubén G. Barrera, Phys. Rev. B **23**, 5707 (1981).

[40] W. Luis Mochán, R. Fuchs, and Rubén G. Barrera, Phys. Rev. B **27**, 771 (1983).

[41] W. Luis Mochán, Rubén G. Barrera, and Ronald Fuchs, Phys. Rev. B **33**, 5350 (1986).

[42] A. A. Maradudin and D. L. Mills, Phys. Rev. B **7**, 2787 (1973).

[43] F. Ercolessi, E. Tosatti, and M. Parrinello, Phys. Rev. Lett. **57**, 719 (1986).

[44] F. Forstmann and H. Stenschke, Phys. Rev. B **17**, 1489 (1978).

[45] F. Forstmann, Z. Phys. B **32**, 385 (1979).

[46] R. Kötz, D. M. Kolb, and F. Forstmann, Surf. Sci. **91**, 489 (1980).

[47] A. D. Boardman and R. Ruppin, Surf. Sci. **112**, 153 (1981).

[48] F. Forstmann and H. Stenschke, Phys. Rev. Lett. **38**, 1365 (1977).

[49] P. Halevi and R. Fuchs, J. Phys. C **17**, 3869 (1984).

[50] P. J. Feibelman, Prog. Surf. Sci. **12**, 287 (1982).

[51] P. J. Feibelman, Phys. Rev. B **12**, 1319 (1975).

[52] G. S. Agarwal, R. B. Barrera, and R. Fuchs, *Proceedings of the International Workshop on the Electromagnetic Response of Surfaces,* edited by R. G. Barrera and W. Luis Mochán (IFUNAM, Mexico, 1984), p. 97.

[53] G. S. Agarwal and C. V. Kunasz, Phys. Rev. B **26**, 5832 (1982).